

Yb-Substitution and Ultralow Thermal Conductivity of the $\text{Ca}_{3-x}\text{Yb}_x\text{AlSb}_3$ ($0 \leq x \leq 0.81(1)$) System

Junsu Lee,¹ Yeongjin Hong,¹ Donghwan Seo,¹ Philip Yox,^{2,4} Myung-Ho Choi,³ Kang Min
Ok,³ Kirill Kovnir,^{2,4} Gordon J. Miller,² and Tae-Soo You^{1,*}

¹ Department of Chemistry and BK21Four Research Team, Chungbuk National University, Cheongju,
Chungbuk 28644, Republic of Korea

² Department of Chemistry, Iowa State University, Ames, IA 50010, USA

³ Department of Chemistry, Sogang University, Seoul 04107, Republic of Korea

⁴ US Department of Energy Ames National Laboratory, Ames, IA 50011, USA

CORRESPONDING AUTHOR FOOTNOTE

Email: tyou@chungbuk.ac.kr

Phone: +82 (43) 261-2282

Fax: +82 (43) 267-2289

Abstract

A series of Yb-substituted Zintl phases in the $\text{Ca}_{3-x}\text{Yb}_x\text{AlSb}_3$ ($0 \leq x \leq 0.81(1)$) system has been synthesized by arc-melting followed by the post-heat-treatment, and their isotypic crystal structures were determined by both powder and single crystal X-ray diffraction analysis. All four title compounds adopted the Ca_3AlAs_3 -type phase (space group $Pnma$, Pearson code $oP28$, $Z = 4$), and the overall structure can be described as an assembly of the 1-dimensional (1D) infinite chain of $\frac{1}{\infty}[\text{Al}(\text{Sb}_2\text{Sb}_{2/2})]$ formed by the two vertices sharing $[\text{AlSb}_4]$ tetrahedral moieties and the three $\text{Ca}^{2+}/\text{Yb}^{2+}$ mixed-sites located in between those 1D chains. The independency of the 1D chains in the title system was explained by the Zintl-Klemm formalism $[\text{Ca}^{2+}/\text{Yb}^{2+}]_3[(4\text{b-Al}^{1-})(1\text{b-Sb}^{2-})_2(2\text{b-Sb}^{1-})_2/2]$. A series of DFT calculations proved that 1) the band overlap between the d -orbital states from two types of cations and the p -orbital states from Sb at the high symmetry Γ point implied an enhanced metallic behavior of the quaternary $\text{Ca}_2\text{YbAlSb}_3$ model and 2) the site-preference of Yb for the M1-site was due to the electronic-factor criterion based on the Q values of each atomic site. The electron localization function calculations also proved that the two different shapes of lone-pairs of the Sb atoms: the “umbrella-shape” and the “C-shape”, are determined by local geometry and the coordination environment on the anionic frameworks. Thermoelectric measurements of the quaternary title compound $\text{Ca}_{2.19(1)}\text{Yb}_{0.81}\text{AlSb}_3$ showed approximately two times larger ZT value than that of the ternary Ca_3AlSb_3 at 623 K due to the increased electrical conductivity and the ultralow thermal conductivity originated from the Yb-substitution for Ca.

■ INTRODUCTION

Thermoelectric (TE) materials and devices have been considered one of the sustainable energy solutions for the global warming crisis which our modern society confronts since they can directly convert wasted heat from various heat sources into electricity.^{1,2} The efficiency of TE materials is defined by the dimensionless figure-of-merit $ZT = \sigma S^2 T / \kappa$ (σ : electrical conductivity, S : Seebeck coefficient, T : absolute temperature, κ : thermal conductivity),¹ and Zintl phase is one of the best candidates for the TE applications due to its high Seebeck coefficients based on the semiconducting character and low thermal conductivities based on the complex crystal structure.^{3,4} In the last several years, my research group has been exploring various Zintl phase systems for TE material applications, and these include the $\text{Ca}_{5-x-y}\text{Yb}_x\text{Eu}_y\text{Al}_2\text{Sb}_6$,³ $\text{Ca}_{5-x-y}\text{Yb}_x\text{RE}_y\text{Al}_2\text{Sb}_6$ (RE = Pr, Nd, Sm),⁵ $\text{Ba}_{2-x}\text{Sr}_x\text{Zn}_{2-y}\text{Cd}_y\text{Sb}_2$, and $\text{Ca}_{11-x}\text{A}_x\text{Sb}_{10-y}\text{Ge}_y$ (A = Na, Li)⁶ systems. Interestingly, during the recent investigation for the $\text{Ca}_{5-x}\text{Yb}_x\text{Al}_{2-y}\text{In}_y\text{Sb}_6$ ($\text{Ca}_5\text{Ga}_2\text{As}_6$ -type) system,⁷ the other Zintl compound Ca_3AlSb_3 adopting the Ca_3AlAs_3 -type phase was serendipitously obtained as a secondary phase, and due to its structural similarity to the $\text{Ca}_5\text{Ga}_2\text{As}_6$ -type phase and the semiconducting character, we decided to expand our research activity up to the Ca_3AlAs_3 -type quaternary $\text{Ca}_{3-x}\text{Yb}_x\text{AlSb}_3$ system. Interestingly, in both the Ca_3AlAs_3 -type and the $\text{Ca}_5\text{Ga}_2\text{As}_6$ -type phases, the anionic $[\text{AlSb}_4]$ tetrahedral moiety acts like a basic building block to form an infinite one-dimensional (1D) $\infty^1[\text{AlSb}_2\text{Sb}_{2/2}]$ chain via vertex-sharing with its neighbors.⁸ However, in the $\text{Ca}_5\text{Ga}_2\text{As}_6$ -type phase, such two 1D chains are further connected via the Sb-Sb bond to build the dimerized 1D $\infty^1[\text{Al}_2\text{Sb}_4\text{Sb}_{4/2}]$ double chains,³ unlike the title Ca_3AlAs_3 -type phase having each 1 D chain independent.

In this work, the influence of a cationic Yb-substitution for Ca on the crystal structure, electronic structure, and TE properties in the title $\text{Ca}_{3-x}\text{Yb}_x\text{AlSb}_3$ ($0 \leq x \leq 0.81(1)$) system was

thoroughly studied using the experimental and theoretical investigations. Four title compounds were successfully synthesized by the arc-melting and the Pb-metal flux reaction methods, and their isotypic crystal structures were carefully characterized by powder and single-crystal X-ray diffraction (PXRD and SXR) analyses. The structural co-relationship between the title $\text{Ca}_{3-x}\text{Yb}_x\text{AlSb}_3$ (Ca_3AlAs_3 -type) phase and the $\text{Ca}_{5-x}\text{Yb}_x\text{Al}_2\text{Sb}_6$ ($\text{Ca}_5\text{Ga}_2\text{As}_6$ -type) phase⁹ was nicely elucidated by the Zintl-Klemm formalism,¹⁰ and the cationic site-preference over the three available sites in the $\text{Ca}_{3-x}\text{Yb}_x\text{AlSb}_3$ system was explained by the electronic-factor criterion based on the Q value (QVAL) of each site. Moreover, a series of theoretical calculations using the tight-binding linear muffin-tin orbital (TB-LMTO) method confirmed the enhanced electrical conductivity of the Yb-substituted quaternary compound based on the partial and total density of states (PDOS and TDOS) curves and band structures analyses. Electron localization function (ELF) diagrams also proved the different distributions of paired electron density in two structure types. Electrical transport property and thermal conductivity measurements proved that the Yb-substitution for Ca successfully improved the ZT value of the quaternary $\text{Ca}_{2.19(1)}\text{Yb}_{0.81}\text{AlSb}_3$ due to the increased σ and the ultralow κ_{tot} .

■ EXPERIMENTAL SECTION

Synthesis. Four novel title Zintl phase compounds were prepared inside an Ar-filled glovebox with O_2 and H_2O contents below 0.1 ppm or under a vacuum. All elements were purchased from Alfa Aesar: Ca (shot, 99.5%), Yb (ingot, 99.9%), Al (shot, 99.9%), Sb (shot, 99.999%), and Ge (piece, 99.9%). First, the title compounds $\text{Ca}_{3-x}\text{Yb}_x\text{AlSb}_3$ were initially synthesized with the loaded ratio of Ca:Yb:Al:Sb = 3- x : x :1:3 by arc-melting followed by annealing at 1073 K for 1 week.

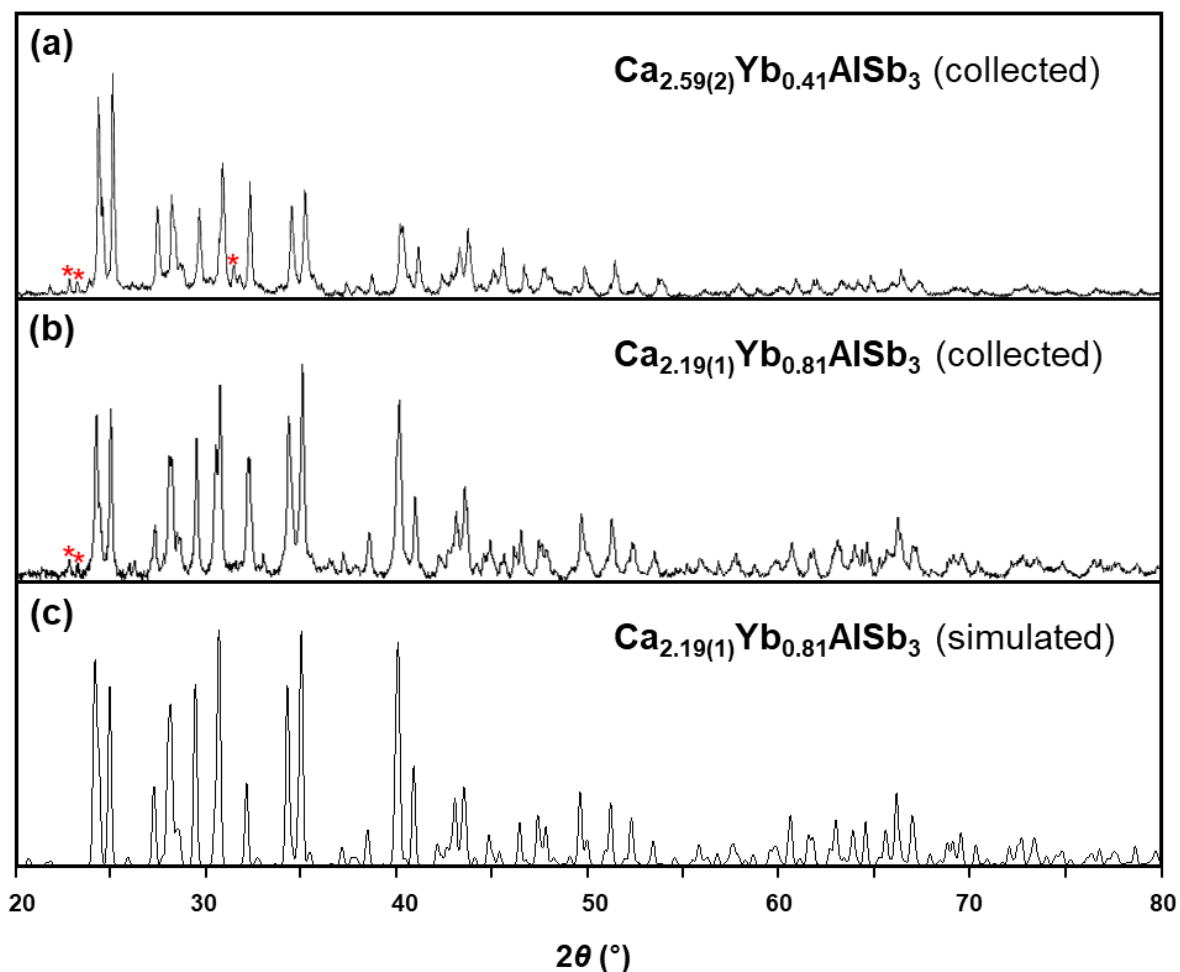


Figure 1. Collected PXRD patterns of the two quaternary title compounds: $\text{Ca}_{2.59(2)}\text{Yb}_{0.41}\text{AlSb}_3$ and $\text{Ca}_{2.19(1)}\text{Yb}_{0.81}\text{AlSb}_3$. A simulated PXRD pattern of $\text{Ca}_{2.19(1)}\text{Yb}_{0.81}\text{AlSb}_3$ is also provided as a reference. Asterisks indicate peaks from a trace amount of the secondary phase $\text{Ca}_{14}\text{AlSb}_{11}$.

The reaction produced a mixture of three phases containing the major phase of $\text{Ca}_{5-x}\text{Yb}_x\text{Al}_2\text{Sb}_6$ and $\text{Ca}_{3-x}\text{Yb}_x\text{AlSb}_3$ with some additions of $\text{Ca}_{14-x}\text{Yb}_x\text{AlSb}_{11}$ according to PXRD analysis. However, as a small amount of Ge was loaded for Sb with the ratio of Ca:Yb:Al:Sb:Ge = 3- x : x :1:2.7:0.3 ($x = 0, 0.5$), the nearly single-phase products were successfully obtained with a trace amount of $\text{Ca}_{14-x}\text{Yb}_x\text{AlSb}_{11}$ as shown in Figure 1 (a). Quite interestingly, according to SXRD analyses, no Ge substitution for Sb was observed in both Ca_3AlSb_3 and

$\text{Ca}_{2.59(2)}\text{Yb}_{0.41}\text{AlSb}_3$. Then, another reaction was also conducted having some Sb-deficiencies rather than the Ge-addition with a loaded ratio of $\text{Ca}:\text{Yb}:\text{Al}:\text{Sb} = 3-x:x:1:2.7$ ($x = 0, 1$) since no Ge was found in the SXRD refinement for two title compounds. As a result, the ternary Ca_3AlSb_3 and the quaternary $\text{Ca}_{2.19(1)}\text{Yb}_{0.81}\text{AlSb}_3$ were successfully obtained according to PXRD (Figure 1(b)) and SXRD analyses.

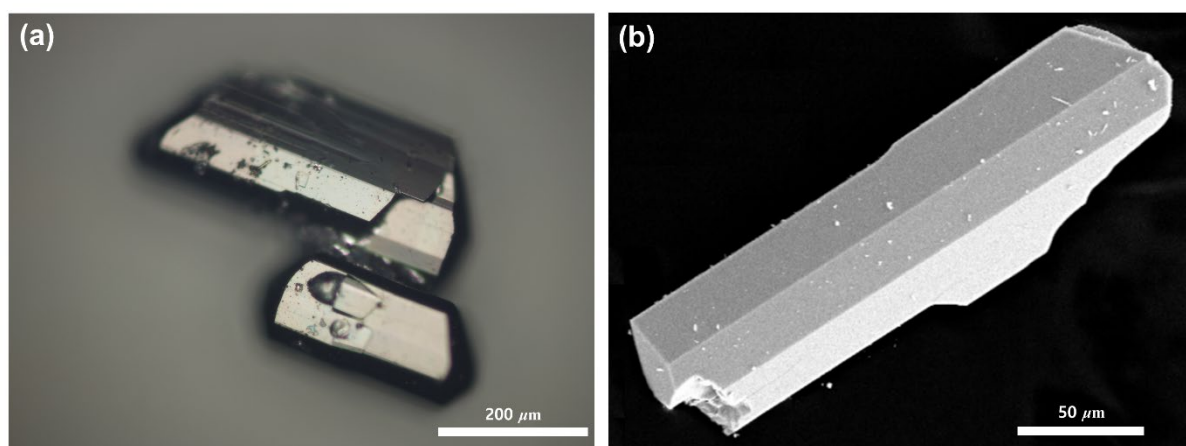


Figure 2. (a) Optical microscopic image and (b) SEM image of single crystals of the quaternary $\text{Ca}_{2.42(1)}\text{Yb}_{0.58}\text{AlSb}_3$ compound. Scale bars are provided.

To grow single crystals, the molten-metal flux method was also exploited using an excess amount of elemental Pb. The reactant mixture and Pb metals were loaded with a ratio of $\text{Ca}:\text{Yb}:\text{Al}:\text{Sb}:\text{Pb} = 2.5:0.5:1:3:30$ in an alumina crucible. In particular, Pb metals were placed on the top and at the bottom of the reactant mixtures, then this alumina crucible was carefully loaded in a fused-silica tube, which was flame sealed under a vacuum. The reaction container was firstly heated up to 960 $^{\circ}\text{C}$ at the rate of 60 $^{\circ}\text{C}/\text{h}$, kept there for 40 h, then cooled down to 500 $^{\circ}\text{C}$ at the rate of 30 $^{\circ}\text{C}/\text{h}$. At this temperature, the reaction container was taken out of the furnace and rapidly centrifuged to separate molten-state Pb metals from the products. As a result, the nicely grown bar-shaped single crystals of $\text{Ca}_{2.42(1)}\text{Yb}_{0.58}\text{AlSb}_3$ were successfully

obtained (See Figure 2).

Caution! Pb used as a flux is a highly poisonous metal. Thus, the molten Pb-metal flux reaction using an excess amount of Pb metal should be executed in a well-ventilated space, and personal protective gear, such as gloves, a goggle, and a mask should be worn during the experiment.

Crystal Structure Determination. Crystal structures and phase purities of the title compounds were characterized by both PXRD and SXRD analyses. Each PXRD pattern was collected at room temperature using a Rigaku Miniflex 600 diffractometer equipped with an area detector and monochromatic Cu K_{α} radiation ($\lambda = 1.54059 \text{ \AA}$). The collection step size was set at 0.02° in the range of $20^{\circ} \leq 2\theta \leq 80^{\circ}$ with a total exposure time of 30 min per sample. The phase purities of these samples were checked by comparing the collected PXRD patterns with the simulated pattern using the SXRD result of $\text{Ca}_{2.19(2)}\text{Yb}_{0.81}\text{AlSb}_3$ as displayed in Figure 1. Two SXRD data of Ca_3AlSb_3 and $\text{Ca}_{2.42(1)}\text{Yb}_{0.58}\text{AlSb}_3$ were collected at room temperature by using a Bruker D8 QUEST diffractometer equipped with Mo $K_{\alpha 1}$ radiation ($\lambda = 0.71073 \text{ \AA}$). A well-grown single crystal was used for full data collection using the APEX3 program.¹¹ The SAINT program¹² was exploited for unit cell parameter refinements, and the SADABS program¹³ was used for semi-empirical absorption corrections based on equivalents. The SXRD data of $\text{Ca}_{2.59(2)}\text{Yb}_{0.41}\text{AlSb}_3$ and $\text{Ca}_{2.19(1)}\text{Yb}_{0.81}\text{AlSb}_3$ were collected at room temperature with synchrotron radiation ($\lambda = 0.65000 \text{ \AA}$) on a Rayonix MX225HS detector at BL2D SMC with silicon (111) double crystal monochromator (DCM) at the Pohang Accelerator Laboratory. For data collection, the PAL BL2D-SMDC program¹⁴ was used, and for data integration and reduction, HKL3000sm (Ver. 716.7)¹⁵ was used. As a result of these refinements, the entire sets of reflections of these title compounds adopted the orthorhombic spacegroup $Pnma$. Further detailed crystal structures were solved by direct methods and refined to convergence by full-

matrix least-squares methods on F^2 . The refined parameters include the scale factor, the atomic positions with anisotropic displacement parameters (ADP), the extinction coefficients, and the occupancy ratio of the three Ca/Yb mixed-sites. After the structural refinements, all atomic positions were standardized by the STRUCTURE TIDY program.¹⁶ Important crystallographic data, atomic positions with ADPs, and selected interatomic distances are provided in Tables 1-3. All these crystallographic data can be obtained free of charge from The Cambridge Crystallographic Data Centre via www.ccdc.cam.ac.uk/data_request/cif. The depository numbers are as follow: CCDC-2235054 for Ca_3AlSb_3 , CCDC-2235055 for $\text{Ca}_{2.59(2)}\text{Yb}_{0.41}\text{AlSb}_3$, CCDC-2235056 for $\text{Ca}_{2.42(1)}\text{Yb}_{0.58}\text{AlSb}_3$, and CCDC-2235057 for $\text{Ca}_{2.19(1)}\text{Yb}_{0.81}\text{AlSb}_3$

Table 1. SXRD data and structure refinement results for the $\text{Ca}_{3-x}\text{Yb}_x\text{AlSb}_3$ ($0 \leq x \leq 0.81(1)$) system.

| Refined Composition | Ca_3AlSb_3 | $\text{Ca}_{2.59(2)}\text{Yb}_{0.41}\text{AlSb}_3$ | $\text{Ca}_{2.42(1)}\text{Yb}_{0.58}\text{AlSb}_3$ | $\text{Ca}_{2.19(1)}\text{Yb}_{0.81}\text{AlSb}_3$ |
|--|----------------------------|--|--|--|
| Formula weight (g/mol) | 512.47 | 566.98 | 589.25 | 620.17 |
| Space group; Z | | | $Pnma$; 4 | |
| a (Å) | 12.8581(5) | 12.860(3) | 12.8627(9) | 12.857(3) |
| b (Å) | 4.4899(2) | 4.4910(9) | 4.4944(3) | 4.4930(9) |
| c (Å) | 14.2776(6) | 14.263(3) | 14.267(1) | 14.254(3) |
| Volume (Å ³) | 824.27(6) | 823.7(3) | 824.8(1) | 823.4(3) |
| d_{calcd} (g/cm ³) | 4.130 | 4.572 | 4.745 | 5.003 |
| Independent reflections | 1296 | 1099 | 1941 | 774 |
| Data/restraints/parameters | 1189/0/43 | 754/0/46 | 1941/0/46 | 774/0/46 |
| R^a indices ($I > 2\sigma_I$) | R_1 | 0.0147 | 0.0446 | 0.0248 |
| | wR_2 | 0.0211 | 0.1133 | 0.0444 |
| GOF on F^2 | 1.065 | 1.040 | 1.298 | 0.973 |
| Largest differences of peak/hole (e/Å ³) | 0.521/−0.627 | 2.527/−2.039 | 1.006/−1.806 | 2.032/−1.128 |

^a $R_1 = \sum||F_o| - |F_c||/\sum|F_o|$; $wR_2 = (\sum(w(F_o^2 - F_c^2)/\sum(w(F_o^2)^2))^{1/2}$, where $w = 1/(\sigma^2F_o^2 + (A - P)^2 + B - P)$, in which $P = (F_o^2 + 2F_c^2)/3$; A and B—weight coefficients.

Table 2. Atomic coordinates and equivalent isotropic displacement parameters (U_{eq}^a) from the SARDA refinements for the $\text{Ca}_{3-x}\text{Yb}_x\text{AlSb}_3$ ($0 \leq x \leq 0.81(1)$) system.

| Atom | Wyckoff Site | Occupation (Ca ²⁺ /Yb ²⁺) | <i>x</i> | <i>y</i> | <i>z</i> | U_{eq}^a (Å ²) |
|--|--------------|---|-----------|----------|-----------|-------------------------------------|
| Ca ₃ AlSb ₃ | | | | | | |
| M1 ^b | 4 <i>c</i> | 1 | 0.2714(1) | 1/4 | 0.7198(1) | 0.0134(2) |
| M2 ^b | 4 <i>c</i> | 1 | 0.3488(1) | 1/4 | 0.0051(1) | 0.0151(2) |
| M3 ^b | 4 <i>c</i> | 1 | 0.5600(1) | 1/4 | 0.6100(1) | 0.0137(2) |
| Al | 4 <i>c</i> | 1 | 0.0668(1) | 1/4 | 0.2970(1) | 0.0122(2) |
| Sb1 | 4 <i>c</i> | 1 | 0.0392(1) | 1/4 | 0.6492(1) | 0.0116(1) |
| Sb2 | 4 <i>c</i> | 1 | 0.1128(1) | 1/4 | 0.1109(1) | 0.0113(1) |
| Sb3 | 4 <i>c</i> | 1 | 0.2554(1) | 1/4 | 0.3801(1) | 0.0116(1) |
| Ca _{2.59(2)} Yb _{0.41} AlSb ₃ | | | | | | |
| M1 ^b | 4 <i>c</i> | 0.85(1)/0.15 | 0.2719(2) | 1/4 | 0.7205(2) | 0.0150(8) |
| M2 ^b | 4 <i>c</i> | 0.86(1)/0.14 | 0.3494(2) | 1/4 | 0.0052(2) | 0.0161(9) |
| M3 ^b | 4 <i>c</i> | 0.88(1)/0.12 | 0.5600(2) | 1/4 | 0.6103(2) | 0.013(1) |
| Al | 4 <i>c</i> | 1 | 0.0666(3) | 1/4 | 0.2970(1) | 0.012(1) |
| Sb1 | 4 <i>c</i> | 1 | 0.0392(1) | 1/4 | 0.6491(1) | 0.0119(4) |
| Sb2 | 4 <i>c</i> | 1 | 0.1130(2) | 1/4 | 0.1107(1) | 0.0118(4) |
| Sb3 | 4 <i>c</i> | 1 | 0.2554(2) | 1/4 | 0.3803(1) | 0.0117(4) |
| Ca _{2.42(1)} Yb _{0.58} AlSb ₃ | | | | | | |
| M1 ^b | 4 <i>c</i> | 0.79(1)/0.21 | 0.2721(1) | 1/4 | 0.7204(1) | 0.0121(2) |
| M2 ^b | 4 <i>c</i> | 0.81(1)/0.19 | 0.3493(1) | 1/4 | 0.0053(1) | 0.0134(2) |
| M3 ^b | 4 <i>c</i> | 0.82(1)/0.18 | 0.5599(1) | 1/4 | 0.6105(1) | 0.0121(2) |
| Al | 4 <i>c</i> | 1 | 0.0668(2) | 1/4 | 0.2969(2) | 0.0104(2) |
| Sb1 | 4 <i>c</i> | 1 | 0.0394(1) | 1/4 | 0.6493(1) | 0.0101(1) |
| Sb2 | 4 <i>c</i> | 1 | 0.1130(1) | 1/4 | 0.1106(1) | 0.0097(1) |
| Sb3 | 4 <i>c</i> | 1 | 0.2555(1) | 1/4 | 0.3803(1) | 0.0101(1) |
| Ca _{2.19(1)} Yb _{0.81} AlSb ₃ | | | | | | |
| M1 ^b | 4 <i>c</i> | 0.71(1)/0.29 | 0.2723(2) | 1/4 | 0.7207(2) | 0.0151(4) |
| M2 ^b | 4 <i>c</i> | 0.74(1)/0.26 | 0.3494(2) | 1/4 | 0.0053(2) | 0.0155(5) |
| M3 ^b | 4 <i>c</i> | 0.75(1)/0.25 | 0.5599(2) | 1/4 | 0.6106(2) | 0.0149(5) |
| Al | 4 <i>c</i> | 1 | 0.0668(2) | 1/4 | 0.2968(2) | 0.0132(7) |
| Sb1 | 4 <i>c</i> | 1 | 0.0394(1) | 1/4 | 0.6493(1) | 0.0128(2) |
| Sb2 | 4 <i>c</i> | 1 | 0.1131(1) | 1/4 | 0.1106(1) | 0.0122(2) |
| Sb3 | 4 <i>c</i> | 1 | 0.2555(1) | 1/4 | 0.3804(1) | 0.0125(2) |

^a U_{eq} is defined as one-third of the trace of the orthogonalized U_{ij} tensor.^bM = Ca in Ca₃AlSb₃; Ca/Yb mixed-site in the three quaternary compounds.

Table 3. Selected interatomic distances (Å) for the $\text{Ca}_{3-x}\text{Yb}_x\text{AlSb}_3$ ($0 \leq x \leq 0.81(1)$) system.

| Atomic Pair | Bond Distance (Å) | | | |
|----------------------------|----------------------------|--|--|--|
| | Ca_3AlSb_3 | $\text{Ca}_{2.59(2)}\text{Yb}_{0.41}\text{AlSb}_3$ | $\text{Ca}_{2.42(1)}\text{Yb}_{0.58}\text{AlSb}_3$ | $\text{Ca}_{2.19(1)}\text{Yb}_{0.81}\text{AlSb}_3$ |
| M1 ^a -Sb1 | 3.151(1) | 3.161(3) | 3.162(2) | 3.162(2) |
| M1 ^a -Sb2 (× 2) | 3.110(1) | 3.112(2) | 3.114(1) | 3.119(2) |
| M1 ^a -Sb3 (× 2) | 3.225(2) | 3.219(2) | 3.222(2) | 3.218(2) |
| M2 ^a -Sb1 | 3.293(1) | 3.287(3) | 3.294(2) | 3.290(2) |
| M2 ^a -Sb1 (× 2) | 3.368(1) | 3.362(3) | 3.367(2) | 3.362(2) |
| M2 ^a -Sb2 | 3.391(1) | 3.392(3) | 3.391(2) | 3.389(2) |
| M2 ^a -Sb3 (× 2) | 3.165(1) | 3.167(3) | 3.169(2) | 3.169(2) |
| M3 ^a -Sb1 | 3.449(1) | 3.443(4) | 3.438(2) | 3.432(2) |
| M3 ^a -Sb2 | 3.226(2) | 3.225(3) | 3.391(2) | 3.226(2) |
| M3 ^a -Sb2 (× 2) | 3.158(1) | 3.161(2) | 3.162(1) | 3.161(2) |
| M3 ^a -Sb3 (× 2) | 3.271(1) | 3.271(2) | 3.274(2) | 3.270(2) |
| Al-Sb1 (× 2) | 2.737(2) | 2.736(4) | 2.740(2) | 2.739(3) |
| Al-Sb2 | 2.722(2) | 2.723(6) | 2.724(3) | 2.721(3) |
| Al-Sb3 | 2.700(2) | 2.703(6) | 0.703(3) | 2.703(3) |

^aM = Ca in Ca_3AlSb_3 ; Ca/Yb mixed-site in three quaternary compounds.

Electronic Structure Calculations. To understand the influence of the Yb-substitution for Ca in the overall electronic structure of the title compounds, we performed a series of DFT calculations using structural models with idealized compositions of Ca_3AlSb_3 and $\text{Ca}_2\text{YbAlSb}_3$ by TB-LMTO method with the atomic sphere approximation (ASA).¹⁷⁻²⁰ In particular, to apply the quaternary composition of $\text{Ca}_2\text{YbAlSb}_3$ for the structural model, a symmetry of a unit cell was lowered from the refined $Pmna$ to its subgroup $P2_1$. The structural details including lattice parameters and atomic coordinates were extracted from the SXRD data of Ca_3AlSb_3 and $\text{Ca}_{2.19(1)}\text{Yb}_{0.81}\text{AlSb}_3$. Detailed structural information used for the quaternary model is provided in Supporting Information Table S1. All relativistic effects, except spin-orbit coupling, were taken into account using a scalar relativistic approximation. The symmetry of the potential inside each Wigner-Seitz (WS)²¹ sphere was considered spherical, and a combined correction was used to take into account the overlapping part. The radii of the WS sphere were obtained by requiring the overlapping potential to be the best possible approximation to the full potential and were determined by an automatic procedure.²¹ A list of the used WS radii are as follows: Ca = 2.07–2.15 Å, Al = 1.59 Å, and Sb = 1.75–1.80 Å for Ca_3AlSb_3 ; Ca = 2.13–2.15 Å, Yb = 2.07 Å, Al = 1.58 Å, and Sb = 1.75–1.80 Å for $\text{Ca}_2\text{YbAlSb}_3$. The basis sets included 4s, 4p, and 3d orbitals for Ca; 6s, 6p, and 5d orbitals for Yb; 3s, 3p, and 3d orbitals for Al; and 5s, 5p, 5d, and 4f orbitals for Sb. The Ca 4p, Yb 6p, Al 3d, and Sb 5d and 4f orbitals were treated by the Löwdin downfolding technique,²² and the Yb 4f wavefunctions were treated as core functions occupied by 14 electrons. The k -space integrations were conducted by the tetrahedron method,²³ and the self-consistent charge density was obtained using 520 irreducible k -points in the Brillouin zone for Ca_3AlSb_3 and $\text{Ca}_2\text{YbAlSb}_3$, respectively.

Thermogravimetric Analysis (TGA). The thermal stability of $\text{Ca}_{2.19(1)}\text{Yb}_{0.81}\text{AlSb}_3$ was verified by TGA using a TA Instruments SDT2960 thermal analyzer. The sample (*ca.* 20 mg)

was enclosed in an alumina crucible, heated under a continuous N₂ flow from room temperature to 900 K at a rate of 10 K/min, and then cooled to room temperature naturally. The result is provided in Supporting Information Figure S1.

Electrical Transport Property Measurements. The ingots of two title compounds Ca₃AlSb₃ and Ca_{2.19(1)}Yb_{0.81}AlSb₃ were cut and polished into bar-shaped samples (3 mm × 3 mm × 10 mm) for the electrical transport property measurements. The longer direction of the bar-shaped samples coincided with the direction in which the electrical transport property was measured, and the measurements were performed through the cross-plane direction. Both the electrical conductivity σ and Seebeck coefficient S were simultaneously measured under a He atmosphere from 303 to 698 K using a ULVAC-RIKO ZEM-3 instrument system.

Thermal Conductivity Measurements. Thermal diffusivity (D) was measured for a disk-shaped sample of Ca_{2.19(1)}Yb_{0.81}Al₂Sb₆ under the Ar atmosphere from 298 K to 673 K by a flash diffusivity method using a Netzsch LFA 467 HT Hyper Flash instrument. In the flash diffusivity method, the front face of the disk was irradiated by a short energy light pulse, and the resultant temperature change on the rear face was recorded and analyzed by an IR detector. Then, the thermal conductivity κ was calculated using the equation $\kappa = DC_p\rho$ (D : thermal diffusivity, C_p : heat capacity, ρ : density), where the Dulong-Petit value ($3R/\text{atom}$, R = gas constant) was used for C_p .²⁴ In general, the total thermal conductivity κ_{tot} can be evaluated by the summation of the lattice thermal conductivities κ_{latt} and the electronic thermal conductivities κ_{elec} .²⁴ In particular, κ_{elec} can be calculated by the Wiedemann-Franz law $\kappa_{\text{elec}} = L\sigma T$ (L : the temperature-dependent Lorenz number), where an L value is estimated using the single parabolic band model from the temperature-dependent Seebeck coefficient S .²⁴ Therefore, κ_{latt} was simply calculated from an equation $\kappa_{\text{latt}} = \kappa_{\text{tot}} - \kappa_{\text{elec}}$.

SEM Images. Several nicely grown single crystals were carefully hand-picked and loaded

on an aluminum puck using conducting carbon tape inside an Ar-filled glovebox. An enhanced image of the best single crystal with a bar-shape was taken by using an ULTRA Plus field-emission scanning electron microscope (SEM) system with an acceleration voltage of 30 kV (Figure 2(b)).

■ RESULT AND DISCUSSION

Crystal Structure Analysis. Four Zintl phase solid solutions in the $\text{Ca}_{3-x}\text{Yb}_x\text{AlSb}_3$ ($0 \leq x \leq 0.81(1)$) system have been successfully synthesized by arc-melting followed by annealing at an elevated temperature. The Pb-metal flux reaction method using the excess amount of elemental Pb as an inactive flux was also conducted to grow large bar-shaped single crystals (Figure 2). Phase purities of the title compounds were checked by PXRD analysis as shown in Figure 1, and a trace amount of the $\text{Ca}_{14}\text{AlSb}_{11}$ phase was observed, similar to reports for other articles analogous Zintl phases, such as Ca_3AlSb_3 ,⁸ $\text{Ca}_{3-x}\text{Na}_x\text{AlSb}_3$,²⁵ and $\text{Ca}_3\text{Al}_{1-x}\text{Zn}_x\text{Sb}_3$.²⁶ The further structural details including the lattice parameters, atomic coordinates, and the mixed occupations of Ca^{2+} and Yb^{2+} were thoroughly refined by using SXRD data. These refinement results proved that the four title compounds adopted the Ca_3AlAs_3 -type phase²⁷ having the orthorhombic *Pnma* (Pearson code *oP28*, $Z = 4$) space group with a total of seven crystallographically independent atomic sites: three Ca/Yb mixed-sites, one Al site, and three Sb sites as provided in Tables 1-3.

The overall crystal structure of the title $\text{Ca}_{3-x}\text{Yb}_x\text{AlSb}_3$ system can be viewed as an assembly of a single $[\text{AlSb}_4]$ tetrahedron moiety (Figure 3(a)) in such a way that each $[\text{AlSb}_4]$ moiety acts as a basic building block to form the 1D infinite chain of $\frac{1}{\infty}[\text{Al}(\text{Sb}_2\text{Sb}_{2/2})]$ by sharing its two vertices with two neighboring identical tetrahedra shown in Figure 3(b).

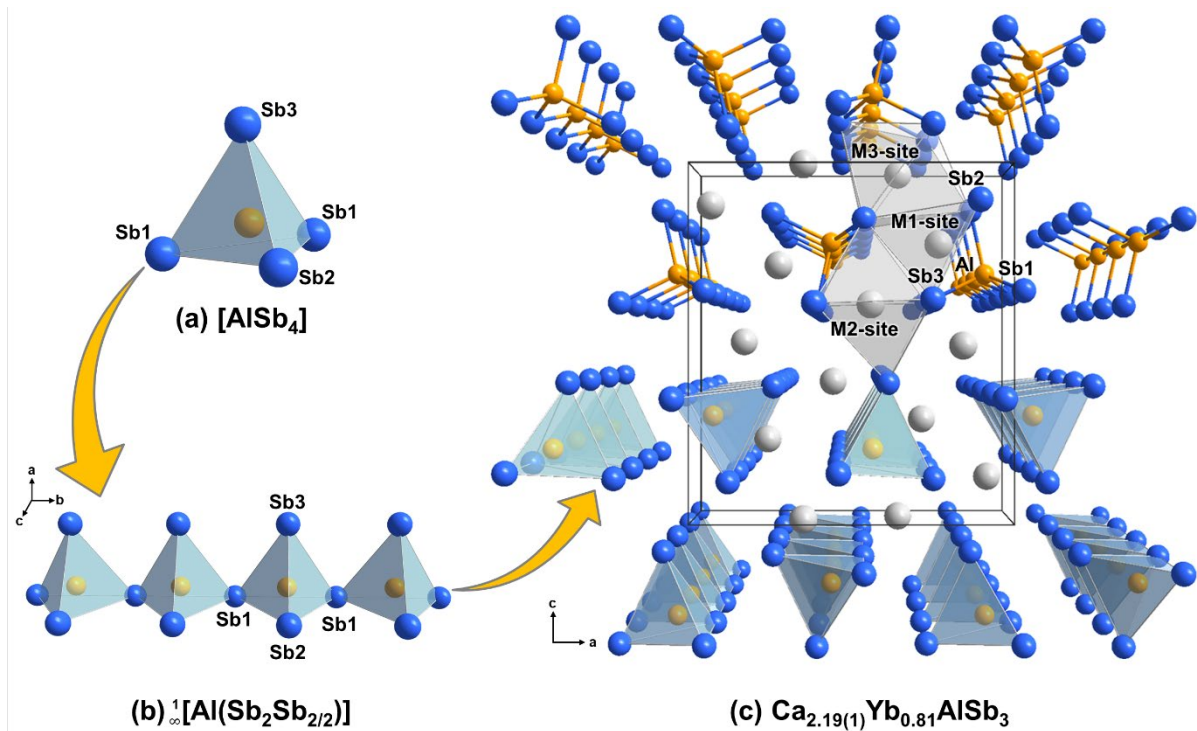
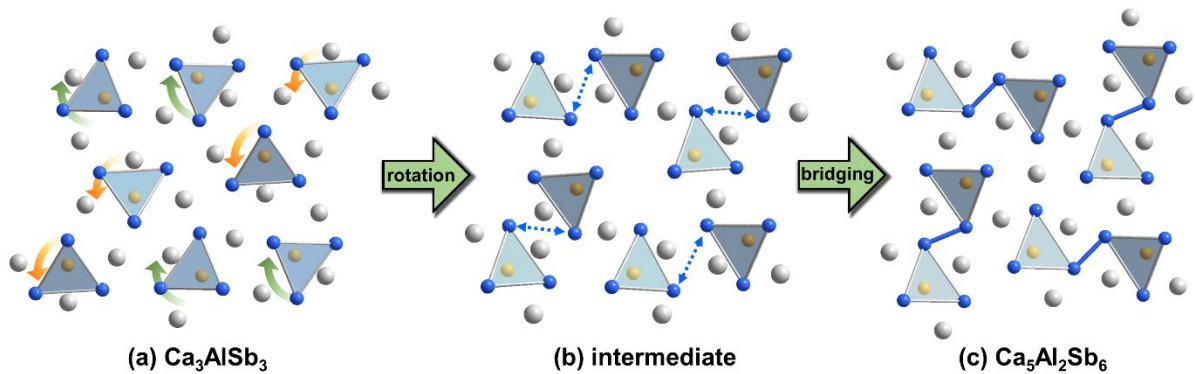


Figure 3. The crystal structure of the quaternary $\text{Ca}_{2.19(1)}\text{Yb}_{0.81}\text{AlSb}_3$ described as a combination of ball-and-stick and polyhedral representations. The overall crystal structure can be viewed as an assembly of (a) a tetrahedral $[\text{AlSb}_4]$ moiety forming (b) the discrete 1D ${}^1_{\infty}[\text{Al}(\text{Sb}_2\text{Sb}_{2/2})]$ chain propagating along the b -axis direction resulting in (c) the Ca_3AlAs_3 -type structure. Color code: M (Ca/Yb mixed-site), light gray; Al, orange; Sb, blue.

Quite interestingly, this type of tetrahedral $[\text{AlSb}_4]$ building blocks and the 1D chains are often observed in other Zintl phase compounds including the $\text{Ca}_{5-x}\text{Yb}_x\text{Al}_2\text{Sb}_6$ ⁹ and the $\text{Ca}_{5-x-y}\text{Yb}_x\text{RE}_y\text{Al}_2\text{Sb}_6$ (RE = Pr, Nd, and Sm)⁵ systems adopting either the $\text{Ca}_5\text{Ga}_2\text{As}_6$ -type²⁸ or the $\text{Ca}_5\text{Al}_2\text{Bi}_6$ -type⁸ structures. However, in those structure types, the 1D ${}^1_{\infty}[\text{Al}(\text{Sb}_2\text{Sb}_{2/2})]$ chains are not discrete as observed in the title compounds, instead they are further connected to their identical neighbors by forming the bridging Sb-Sb bonds between two 1D chains resulting in the slightly different 1D ${}^1_{\infty}[\text{Al}_2(\text{Sb}_4\text{Sb}_{4/2})]$ double chains. This kind of similar, but distinctive local connectivity of the 1D chains in the title $\text{Ca}_{3-x}\text{Yb}_x\text{AlSb}_3$ system can be rationalized by the

Zintl-Klemm formalism¹⁰: $[\text{Ca}^{2+}/\text{Yb}^{2+}]_3[(4\text{b-Al}^{1-})(1\text{b-Sb}^{2-})_2(2\text{b-Sb}^{1-})_{2/2}]$. By the doubling of the number of formula units in a unit cell, the composition of the title compound can be re-written as $\text{Ca}_{6-x}\text{Yb}_x\text{Al}_2\text{Sb}_6$ ($= \text{Ca}_{3-x}\text{Yb}_x\text{AlSb}_3 \times 2$). Then, we now realize that one additional divalent cation (compared to $\text{Ca}_{5-x}\text{Yb}_x\text{Al}_2\text{Sb}_6$) can donate two more electrons to the anionic frameworks in the title Ca_3AlAs_3 -type structure, and as a result, the 1-bonded vertex Sb atoms on the 1D chains don't need to share electrons with the Sb neighbors to fulfill the Zintl-Klemm formalism as occurred in the $\text{Ca}_5\text{Ga}_2\text{As}_6$ -type²⁸ or $\text{Ca}_5\text{Al}_2\text{Bi}_6$ -type⁸ structures. Therefore, we only see the discrete 1D anionic chains propagating along the b -axis direction as illustrated in Figure 3(c).



Scheme 1. Schematic illustration showing the structural transformation of $\text{Ca}_{3-x}\text{Yb}_x\text{AlSb}_3$ (Ca_3AlAs_3 -type) to $\text{Ca}_{5-x}\text{Yb}_x\text{Al}_2\text{Sb}_6$ ($\text{Ca}_5\text{Ga}_2\text{As}_6$ -type). (a) The discrete 1D chains rotate (counter) clock-wise directions along the b -axis direction, (b) a particular vertex of the tetrahedra on different 1D chains moves close to each other, and (c) the bridging Sb1-Sb1 bond forms completing the $\text{Ca}_5\text{Ga}_2\text{As}_6$ -type $\text{Ca}_5\text{Al}_2\text{Sb}_6$ structure.

In addition, quite interestingly, this $\text{Ca}_5\text{Ga}_2\text{As}_6$ -type $\text{Ca}_{5-x}\text{Yb}_x\text{Al}_2\text{Sb}_6$ system⁹ can be derived from our Ca_3AlAs_3 -type title compound structure. As illustrated in Scheme 1(a), 1) the 1D $\frac{1}{\infty}[\text{Al}(\text{Sb}_2\text{Sb}_{2/2})]$ chains in the Ca_3AlAs_3 -type $\text{Ca}_{3-x}\text{Yb}_x\text{AlSb}_3$ are rotated along the clockwise or anticlockwise direction, 2) the vertices of the $[\text{AlSb}_4]$ tetrahedra on these 1D chains come close to each other (Scheme 1(b)), and then 3) at a certain point when those vertices are close

enough to be connected, they form inter Sb-Sb bond between two 1D chains while the 1/6 of Ca cations are removed (Scheme 1(c)), which eventually results in forming the $\text{Ca}_5\text{Ga}_2\text{As}_6$ -type $\text{Ca}_{5-x}\text{Yb}_x\text{Al}_2\text{Sb}_6$.⁹

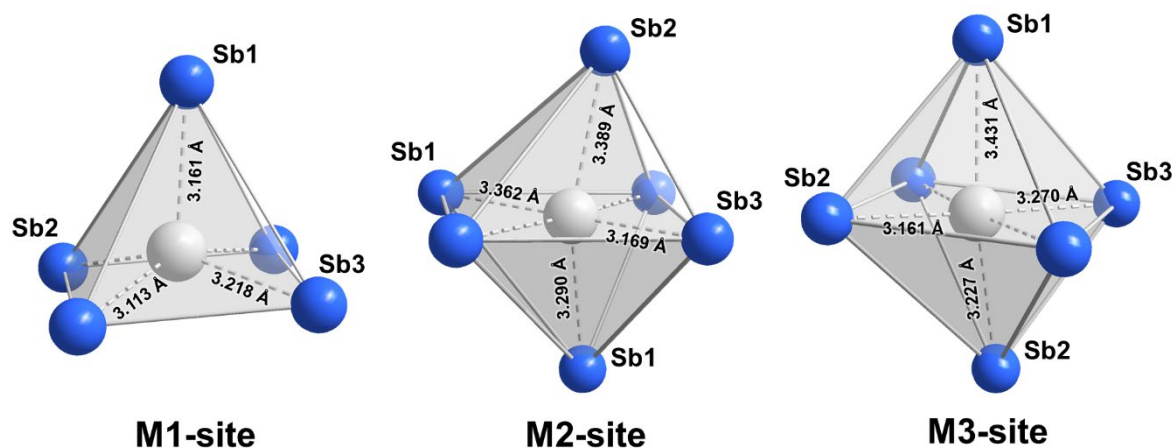


Figure 4. Three different cationic sites surrounded by Sb atoms in $\text{Ca}_{2.19(1)}\text{Yb}_{0.81}\text{AlSb}_3$. Selected atomic labels and interatomic distances are provided.

Figure 4 illustrates the three different cationic sites surrounded by five or six Sb atoms. In particular, the M1-site is surrounded by five Sb atoms forming a square-pyramidal environment, whereas the M2-site and the M3-site are surrounded by six Sb atoms forming the distorted octahedral coordination environment. Interestingly, these three cationic sites show the site-preference of cationic Ca^{2+} and Yb^{2+} , where the largest Yb^{2+} occupation is observed at the M1-site in all three quaternary title compounds. Due to the similar cationic sizes of Ca^{2+} and Yb^{2+} ($r(\text{Ca}^{2+}) = 1.00 \text{ \AA}$, $r(\text{Yb}^{2+}) = 1.02 \text{ \AA}$),²⁹ the size-factor criterion cannot elucidate this phenomenon, but the electronic-factor criterion based on the QVAL of an atomic site and the electronegativity of an atom occupying the site should explain this type of site-preference.^{30,31} We will further discuss the site-preference based on the electronic-factor in the Electronic

Structure Analysis section.

Electronic Structure Analysis. To understand the influence of Yb-substitution for Ca on the electronic structure of the title $\text{Ca}_{3-x}\text{Yb}_x\text{AlSb}_3$ system, a series of DFT calculations were conducted by the TB-LMTO-ASA method¹⁷⁻²⁰ using the two structural models. For practical reasons, the idealized compositions of Ca_3AlSb_3 for the ternary compound and $\text{Ca}_2\text{YbAlSb}_3$ for the quaternary compound were exploited. In addition, the space group for the quaternary $\text{Ca}_2\text{YbAlSb}_3$ was lowered from the experimentally refined *Pmna* to its subgroup *P2₁* to properly apply the idealized composition. The structural details including lattice parameters and atomic coordinates were extracted from the SXRD refinement result of Ca_3AlSb_3 and $\text{Ca}_{2.19(1)}\text{Yb}_{0.81}\text{AlSb}_3$ for each model.

TDOS and PDOS curves of these two models are very similar and indicate the overall strong orbital mixings throughout the entire energy range (Figure 5(a) and (c)). In particular, in DOS curves of $\text{Ca}_2\text{YbAlSb}_3$ (Figure 5(c)), 1) the low energy region between *ca.* -10.5 and -8.5 eV below the Fermi level (E_F) mostly contains the *s*-orbital states of Al and Sb, 2) the region between -6.1 and -4.8 eV shows the large contributions from the *p*-orbital states of Sb1 atoms, and 3) the region from *ca.* -4.8 eV to E_F includes the *p*-orbital states of Al, Sb2, and Sb3 atoms with some contributions from the cationic elements. Interestingly, as the amount of Yb substituent increased, the DOS near the E_F also slightly increased as compared in Figure 5(a) and (c). Such an increase in DOS level should directly affect the electrical transport properties, and in fact, the overall electrical conductivity of the quaternary $\text{Ca}_{2.19(1)}\text{Yb}_{0.81}\text{AlSb}_3$ is improved compared to that of the ternary Ca_3AlSb_3 . We will further discuss these changes in electrical transport property in the subsequent Physical Property Measurements section.

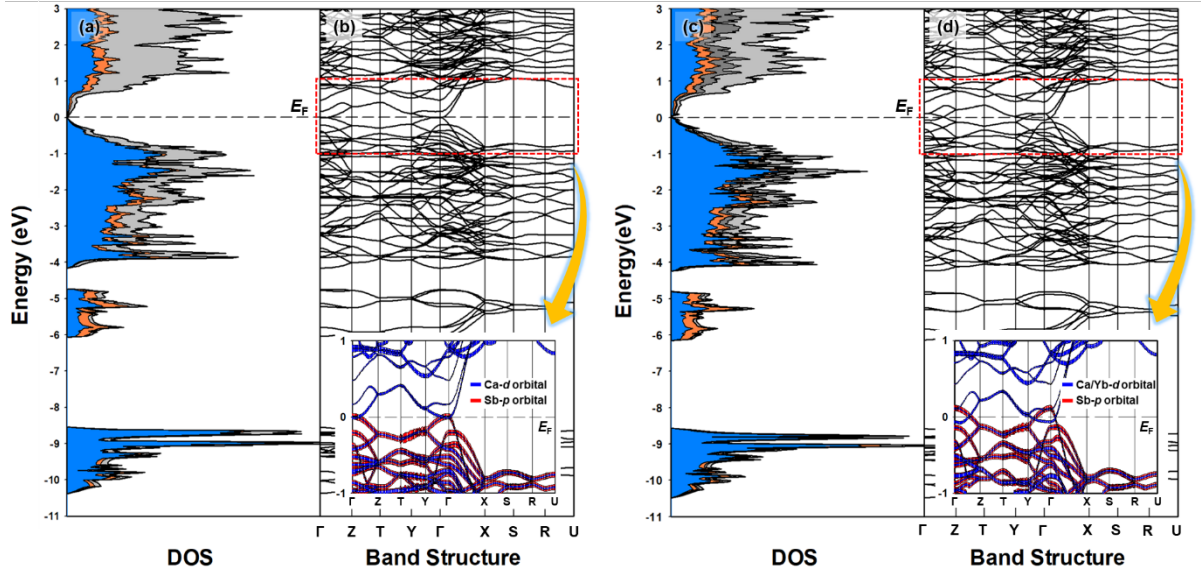


Figure 5. TDOS, PDOS, and band structure of Ca_3AlSb_3 ((a), (b)) and $\text{Ca}_2\text{YbAlSb}_3$ ((c), (d)). Color codes in DOS curves are as follows: TDOS, bold black outline; Ca PDOS, gray region; Yb PDOS, dark gray region; Al PDOS, orange region; and Sb PDOS, blue region. E_F (horizontal dashed line) is set as the energy reference at 0 eV. Each inset shows an enlarged energy range between -1 and 1 eV.

The two band structures displayed in Figure 5(b) and (d) also imply the enhancement of electrical transport property caused by the Yb-substitution. In Figure 5(b), the bottom of a conduction band composed of the 3d-orbital states of Ca slightly touches E_F at the high-symmetry point Γ , where the top of the valence band consisting of the p-orbital states of Sb also nearly meets E_F at this special symmetry point. Since the TB-LMTO-ASA method is known to underestimate a band gap size,^{32,33} we could expect to see a semiconducting behavior for Ca_3AlSb_3 . On the other hand, in the quaternary $\text{Ca}_2\text{YbAlSb}_3$ compound, the 3d/5d-orbital states of Ca and Yb come down and across E_F , and the p-orbital states of Sb also move up and across E_F resulting in a certain amount of band overlapping at this special symmetry point Γ . This kind of orbital overlapping implies a metallic behavior for our quaternary compound, and these theoretical investigations are in quite good agreement with the electrical conductivities

of the title compounds, which we will discuss in the subsequent section.

Table 4. QVAL of each atomic site in Ca_3AlSb_3 .

| Atom | Ca1 | Ca2 | Ca3 | Al | Sb1 | Sb2 | Sb3 |
|------|-------|-------|-------|-------|-------|-------|-------|
| QVAL | 2.404 | 2.352 | 2.361 | 2.659 | 4.863 | 4.710 | 4.652 |

As briefly mentioned in the Crystal Structure Analysis section, the cationic site-preference in the title quaternary compounds should be explained by the electronic-factor criterion based on the QVAL of each atomic site. In general, the more electronegative element prefers to occupy the atomic site having the larger QVAL, where the higher electron density is observed.^{30,31} According to our evaluations for the QVAL, the M1-site offers the largest QVAL among the three available sites as shown in Table 4. Therefore, the largest Yb occupation at the M1-site can be rationalized by the electronic-factor criterion (electronegativity of Ca = 1.04 vs. Yb = 1.06 in the Allred-Rochow scale).³⁴ Sites M2 and M3 have similar QVAL values and site occupancies of Yb in those sites are very close (Table 2).

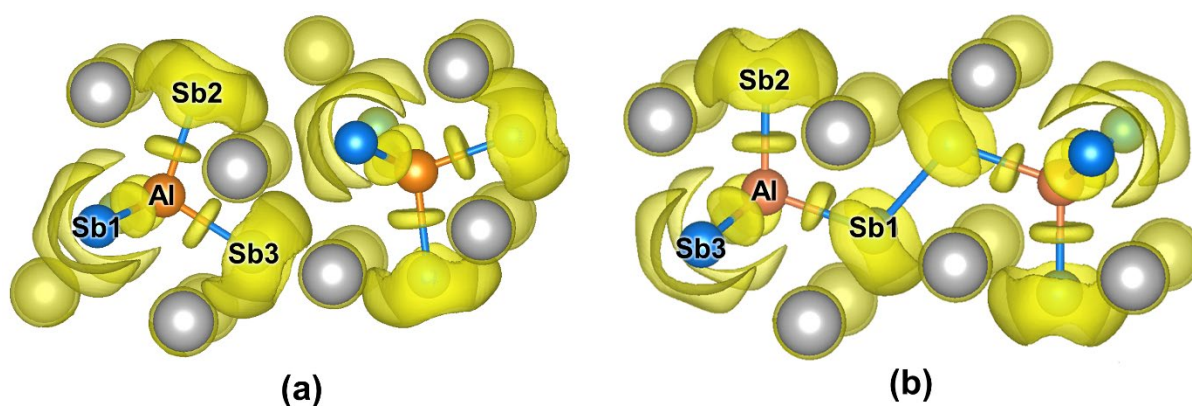


Figure 6. The 3D isosurfaces of ELF illustrating lone-pairs and bonding-pairs of electrons in the coordination geometries of (a) the discrete $[\text{AlSb}_4]$ tetrahedra in Ca_3AlSb_3 and (b) the dimerized $[\text{Al}_2\text{Sb}_8]$ unit in $\text{Ca}_5\text{Al}_2\text{Sb}_6$. The isosurfaces show the area with ELF values of 0.65. Color code: Ca/Yb mixed-unit.

site, light gray; Al, orange; and Sb, blue.

Chemical bonding in Ca_3AlSb_3 and the stereotypic $\text{Ca}_5\text{Al}_2\text{Sb}_6$ was analyzed by means of Electron Localization Function (ELF) analysis. ELF isosurfaces were carefully compared to each other to understand the distributions of paired-electron densities within the anionic frameworks. In particular, as nicely illustrated in Figure 6 (a), two terminal Sb atoms (Sb2 and Sb3) in Ca_3AlSb_3 show a kind of “umbrella-shaped” paired-electron densities representing three lone-pairs to the opposite side of bonding-pairs. Analogously ELF isosurfaces were observed for other 1-bonded main group elements, such as Se_2^{2-} or Sb_3^{7-} . [Wang, J.; Lee, K.; Kovnir, K. Synthesis, crystal and electronic structure, and optical properties of two new chalcogenide-iodides: $\text{Ba}_3\text{Q}_4\text{I}_2$ (Q = S, Se). *Inorg. Chem. Front.* 2016, 3, 306-312; Hu, Y.; Wang, J.; Kawamura, A.; Kovnir, K.; Kazlarich, S.M. $\text{Yb}_{14}\text{MgSb}_{11}$ and $\text{Ca}_{14}\text{MgSb}_{11}$ - New Mg-Containing Zintl Compounds and Their Structures, Bonding and Thermoelectric Properties. *Chem. Mater.* 2015, 27, 343-351.] However, the Sb1 shared by two neighboring Al atoms displays the “C-shaped” paired-electron densities representing two lone-pairs of electrons. On the other hand, in the ELF diagram of $\text{Ca}_5\text{Al}_2\text{Sb}_6$ (Figure 6(b)), the terminal Sb2 atoms still display the umbrella-shaped lone-pairs, while the Sb1 atom forming a bridging bond to the other neighboring 1D anionic chains shows the “C-shaped” lone-pairs just like those of Sb3 atoms in Ca_3AlSb_3 . Therefore, we can clearly differentiate the distribution of the electron lone-pairs around the Sb atom forming $[\text{AlSb}_4]$ in two distinctive crystal structures. In addition, the four “disk-shaped” isosurfaces representing bonding pairs of electrons are clearly observed between the central Al and four surrounding Sb atoms. Thus, we can conclude that as an Sb atom occupies the terminal position, it forms the umbrella-shaped lone-pairs of electrons, whereas as an Sb atom is located at the bridging positions, it forms the C-shaped lone-pairs of

electrons.

Thermoelectric Property Measurements. To investigate the effect of Yb-substitution for Ca on the thermoelectric properties in the title $\text{Ca}_{3-x}\text{Yb}_x\text{AlSb}_3$ system, a series of thermoelectric property measurements were performed for the ternary Ca_3AlSb_3 and the quaternary $\text{Ca}_{2.19(1)}\text{Yb}_{0.81}\text{AlSb}_3$. The electrical conductivity and Seebeck coefficient were measured in the temperature range between 303 and 698 K for both compounds, while the thermal conductivity was measured in the temperature between 298 and 673 K only for the quaternary $\text{Ca}_{2.19(1)}\text{Yb}_{0.81}\text{AlSb}_3$ and the values for the ternary Ca_3AlSb_3 were extracted from literature.²⁵

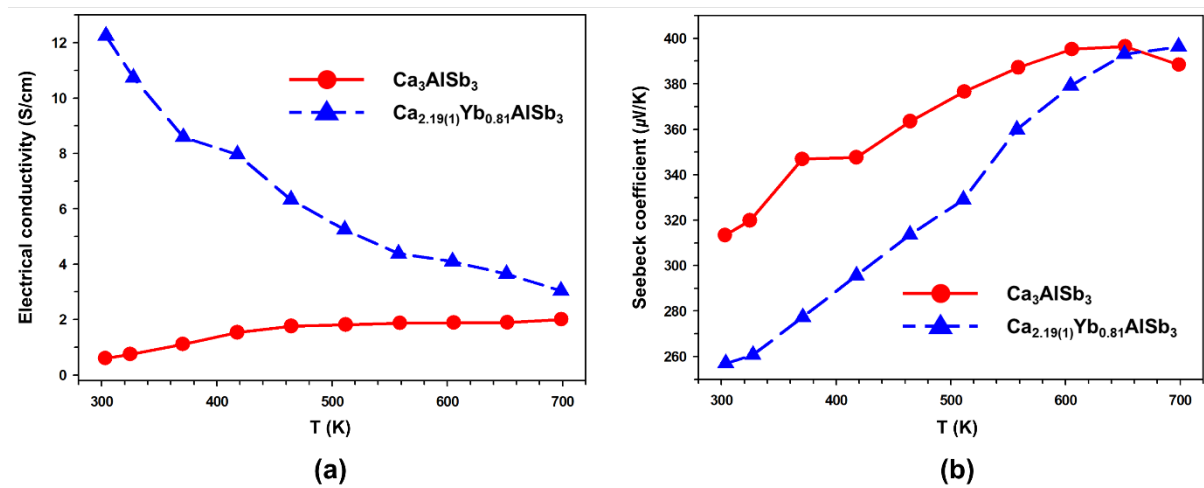


Figure 7. Temperature-dependent (a) electrical conductivity σ and (b) Seebeck coefficient S of Ca_3AlSb_3 and $\text{Ca}_{2.19(1)}\text{Yb}_{0.81}\text{AlSb}_3$ measured between 303 and 698 K.

Temperature-dependent electrical conductivities σ of two compounds are provided in Figure 7 (a). The ternary Ca_3AlSb_3 shows the semiconducting behavior where σ increases with temperature. On the other hand, the quaternary $\text{Ca}_{2.19(1)}\text{Yb}_{0.81}\text{AlSb}_3$ displays a typical metallic property where σ decreases as temperature increases although the absolute σ values of both

compounds are still small. These different σ behaviors of two title compounds are in good agreement with the TDOS curves and band structures as well since as the Yb substituents are introduced in the title $\text{Ca}_{3-x}\text{Yb}_x\text{AlSb}_3$ system, the bandgap size decreases eventually resulting in becoming a poor-metallic compound. The measured σ values of Ca_3AlSb_3 and $\text{Ca}_{2.19(1)}\text{Yb}_{0.81}\text{AlSb}_3$ at room temperature are 0.60 and 12.25 S/cm, respectively, and the larger σ values of the Yb-substituted $\text{Ca}_{2.19(1)}\text{Yb}_{0.81}\text{AlSb}_3$ than those of Ca_3AlSb_3 can be understood based on the electronegativity difference between Yb and Ca (Yb = 1.06; Ca = 1.04 in the Allred-Rochow scale).³⁴ Due to the slightly higher electronegativity of Yb than Ca, as the Yb atom was introduced to the system, a relatively smaller number of electrons were transferred from cationic elements to the anionic frameworks resulting in the increase of hole carrier concentration in $\text{Ca}_{2.19(1)}\text{Yb}_{0.81}\text{AlSb}_3$. A similar type of electrical conductivity enhancement due to the Yb substitution for Ca was already observed in some other Zintl phases TE materials including $\text{Ca}_{1-x}\text{Yb}_x\text{Cd}_2\text{Sb}_2$,³⁵ $\text{Ca}_{1-x}\text{Yb}_x\text{Sb}_{10}$,³⁶ and $\text{Yb}_{13-x}\text{Ca}_x\text{BaMgSb}_{11}$.³⁷

Figure 7 (b) shows the temperature dependences of the Seebeck coefficients S of the title compounds. Due to the inversely proportional relationship of S to σ , S values of the ternary Ca_3AlSb_3 are higher than those of the quaternary $\text{Ca}_{2.19(1)}\text{Yb}_{0.81}\text{AlSb}_3$ up to *ca.* 650 K where these values cross over. The S values of Ca_3AlSb_3 and $\text{Ca}_{2.19(1)}\text{Yb}_{0.81}\text{AlSb}_3$ are 313 and 257 $\mu\text{V/K}$ at room temperature and reach their maximum values of 396 and 396 $\mu\text{V/K}$ at 652 and 698 K, respectively. For semiconducting Ca_3AlSb_3 the temperature dependence of Seebeck coefficient exhibits a clear maximum at 652 K. Estimation of the bandgap from a Goldsmid-Sharp relation as $E_g = 2e|S_{max}|T_{max}$ resulted in the bandgap of 0.52 eV for Ca_3AlSb_3 . [Goldsmid, H. J.; Sharp, J. W. Estimation of the Thermal Band Gap of a Semiconductor from Seebeck Measurements *J. Electron. Mater.* **1999**, 28, 869-872]

The smaller S values of the quaternary $\text{Ca}_{2.19(1)}\text{Yb}_{0.81}\text{AlSb}_3$ than those of the ternary

Ca_3AlSb_3 could be attributed to the increased hole carrier concentration of $\text{Ca}_{2.19(1)}\text{Yb}_{0.81}\text{AlSb}_3$ influenced by the Yb substituents having the higher electronegativity as mentioned earlier. This kind of correlation between S and the carrier concentration can be understood based on the following equation: $S = \frac{8\pi^2 k_B^2}{3eh^2} m^* T \left(\frac{\pi}{3n}\right)^2$, where n is the carrier concentration.^{1,2}

In Figure 8(a), the temperature-dependent total thermal conductivity κ_{tot} of the quaternary $\text{Ca}_{2.19(1)}\text{Yb}_{0.81}\text{AlSb}_3$ was measured in the temperature range between 298 to 673 K and plotted with that of the ternary Ca_3AlSb_3 extracted from literature. Overall, the κ_{tot} values of the quaternary title compound were significantly lower than those of Ca_3AlSb_3 and reached its lowest value of 0.38 W/m·K at 673 K. The dotted line in Figure 8(a) shows the estimated amorphous limit for the lattice thermal conductivity (κ_{glass}) calculated from Cahill's method.²⁵

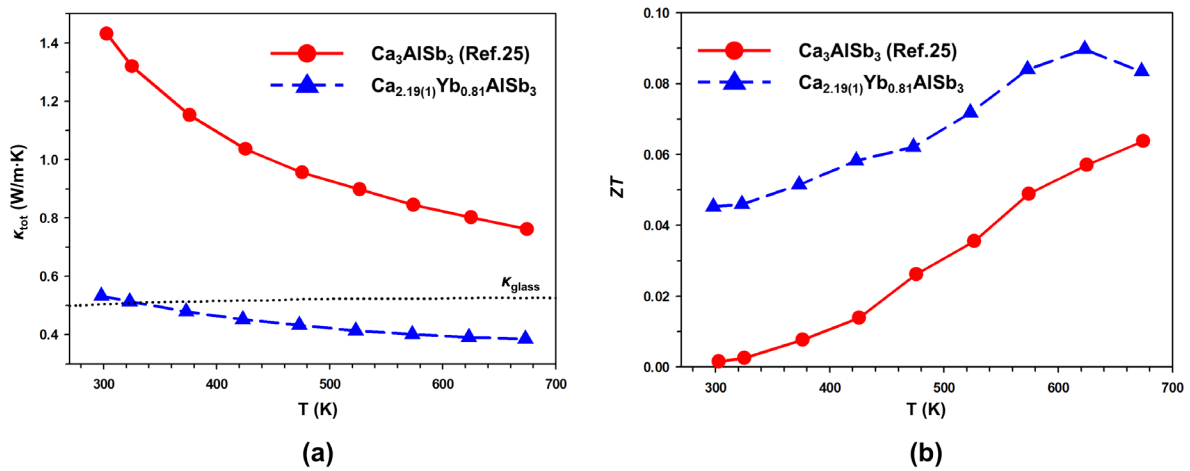


Figure 8. Temperature-dependent (a) total thermal conductivity κ_{tot} and (b) figure-of-merit ZT of $\text{Ca}_{2.19(1)}\text{Yb}_{0.81}\text{AlSb}_3$ measured between 298 and 673 K. The κ_{tot} of Ca_3AlSb_3 is extracted from the literature. The calculated minimum lattice thermal conductivity (κ_{glass}) is also plotted with a dotted line in (a).

This ultralow thermal conductivity of $\text{Ca}_{2.19(1)}\text{Yb}_{0.81}\text{AlSb}_3$ should be attributed to a result

of 1) the complex Ca_3AlAs_3 -type structure and 2) the increased phonon scattering due to the Ca/Yb mixed-occupations at all three cationic sites. This type of low κ_{latt} has been also reported in other Zintl phases including the $\text{Eu}_2\text{Zn}_{1-x}\text{Sb}_2$,³⁸ the $\text{Ca}_9\text{Zn}_{4+x}\text{Sb}_9$,⁴ and the $\text{Yb}_{2-x}\text{Eu}_x\text{CdSb}_2$ ³⁹ systems. In general, κ_{tot} is composed of the electrical contribution term κ_{elec} and the lattice contribution term κ_{latt} , and κ_{elec} can be directly calculated by using the Wiedemann-Franz law ($\kappa_{\text{elec}} = L\sigma T$, $L =$ Lorenz number).²⁴ In the current work, the κ_{elec} of $\text{Ca}_{2.19(1)}\text{Yb}_{0.81}\text{AlSb}_3$ was calculated, and the resultant values were rather insignificant, such as the value of 0.006 W/m·K at 298 K. Therefore, we can conclude that the κ_{latt} term dominates the overall κ_{tot} in the title quaternary compound, and the κ_{latt} is displayed in Supporting Information Figure S2.

As a result of these various TE property measurements, the figure-of-merit ZT values of Ca_3AlSb_3 and $\text{Ca}_{2.19(1)}\text{Yb}_{0.81}\text{AlSb}_3$ can be evaluated (Figure 8 (b)). The maximum ZT value of $\text{Ca}_{2.19(1)}\text{Yb}_{0.81}\text{AlSb}_3$ is 0.090 at 623 K, and this value is about 50% larger than that of Ca_3AlSb_3 , which is 0.063 at 674 K. The improved ZT value of our title compound should be attributed to the increased σ and the ultralow κ_{tot} values originated from the Yb-substitution for Ca. We believe that the further enhancement of ZT for the title $\text{Ca}_{3-x}\text{Yb}_x\text{AlSb}_3$ system could be achieved through electrical engineering by introducing the p -type dopant.²⁵

■ CONCLUSION

Four Zintl phase solid-solutions belonging to the $\text{Ca}_{3-x}\text{Yb}_x\text{Al}_3$ ($0 \leq x \leq 0.81(1)$) system were successfully synthesized, and their crystal structure and TE properties were thoroughly characterized. The title compounds adapted the orthorhombic Ca_3AlAs_3 -type phase, and the overall crystal structure can be described as a combination of 1) the anionic 1D $\infty^1[\text{Al}(\text{Sb}_2\text{Sb}_{2/2})]$ infinite chains propagating along the b -axis direction, and 2) the $\text{Ca}^{2+}/\text{Yb}^{2+}$ -

mixed cationic site in between those 1D chains. Interestingly, the 1D chains in the title system can be distinguished from the 1D $\infty[\text{Al}_2(\text{Sb}_4\text{Sb}_{4/2})]$ double chains previously reported in the stereotypic $\text{Ca}_5\text{Ga}_2\text{As}_6$ -type $\text{Ca}_{5-x}\text{Yb}_x\text{Al}_{2-y}\text{In}_y\text{Sb}_6$ system. This kind of similar, but distinctive connectivities between the neighboring 1D chains can be rationalized by the Zintl-Klemm formalism $[\text{Ca}^{2+}/\text{Yb}^{2+}]_3[(4\text{b}-\text{Al}^{1-})(1\text{b}-\text{Sb}^{2-})_2(2\text{b}-\text{Sb}^{1-})_{2/2}]$ implying that due to the two extra electrons donated from one additional divalent cation in the $\text{Ca}_{3-x}\text{Yb}_x\text{Al}_3$ system, the 1D $\infty[\text{Al}(\text{Sb}_2\text{Sb}_{2/2})]$ chain doesn't need to form the bridging Sb-Sb bond to share the electrons with its neighboring chains. According to the series of DFT calculations, the band overlap between the *d*-orbital states from two types of cations and the *p*-orbital states from Sb at the Γ point indicated an enhanced metallic behavior of the title quaternary $\text{Ca}_2\text{YbAlSb}_3$ compound. The observed site-preference of Ca and Yb in the quaternary compounds should be elucidated by the electronic factor criterion based on the match between the QVAL of an atomic site and the electronegativity of an atom occupying the site. ELF analysis also proved that the shape of lone-pairs of the Sb atoms on the 1D anionic chain in $\text{Ca}_2\text{YbAlSb}_3$ was determined by the local geometry and the coordination environment: the terminal Sb showed the “umbrella-shaped” lone pairs, whereas the bridging Sb formed the “C-shaped” lone-pairs. TE property measurements proved that a quaternary $\text{Ca}_{2.19(1)}\text{Yb}_{0.81}\text{AlSb}_3$ showed approximately four times larger *ZT* value than that of the ternary Ca_3AlSb_3 at 623 K due to the increased σ and the ultralow κ_{tot} originated from the Yb-substitution for Ca.

■ ASSOCIATED CONTENT

Supporting Information

The Supporting Information is available free of charge at <https://pubs.acs.org/doi/10.1021/acs.cgd.XXXXXXX>.

Detailed structural information of two models of Ca_3AlSb_3 and $\text{Ca}_2\text{YbAlSb}_3$, TGA measurement result of $\text{Ca}_{2.19(1)}\text{Yb}_{0.81}\text{AlSb}_3$, and temperature-dependent lattice thermal conductivity κ_{latt} of $\text{Ca}_{2.19(1)}\text{Yb}_{0.81}\text{AlSb}_3$.

Accession Codes

CCDC 2235054-2235057 contain the supplementary crystallographic data for this article.

These data can be obtained free of charge via www.ccdc.ac.uk/data_request/cif, or by emailing data_request@ccdc.cam.ac.uk, or by contacting The Cambridge Crystallographic Data Centre, 12 Union Road, Cambridge CB2 1EZ, UK; fax: +44 1223 336033.

■ AUTHOR INFORMATION

Corresponding Author

Tae-Soo You – *Department of Chemistry and BK21Plus Research Team, Chungbuk National University, Cheongju, Chungbuk 28644, Republic of Korea*; orcid.org/0000-0001-9710-2166;
Phone: +82 (43) 261-2282; Email: tsyou@chungbuk.ac.kr; Fax: +82 (43) 267-2289

Authors

Junsu Lee – *Department of Chemistry and BK21Plus Research Team, Chungbuk National University, Cheongju, Chungbuk 28644, Republic of Korea*; orcid.org/0000-0002-8869-024X

Yeongjin Hong – *Department of Chemistry and BK21Plus Research Team, Chungbuk National University, Cheongju, Chungbuk 28644, Republic of Korea*

Donghwan Seo – *Department of Chemistry and BK21Plus Research Team, Chungbuk National*

University, Cheongju, Chungbuk 28644, Republic of Korea; orcid.org/0000-0003-1559-6436

Philip Yox – *Department of Chemistry, Iowa State University, Ames, Iowa 50011, United States;*

US DOE Ames National Laboratory, Ames, Iowa 50011, United States; orcid.org/ 0000-0002-8524-8202

Myung-Ho Choi – *Department of Chemistry, Sogang University, Seoul 04107, Republic of Korea*

Kang Min Ok – *Department of Chemistry, Sogang University, Seoul 04107, Republic of Korea; orcid.org/0000-0002-7195-9089*

Kirill Kovnir – *Department of Chemistry, Iowa State University, Ames, Iowa 50011, United States; Ames National Laboratory, U.S. Department of Energy, Ames, Iowa 50011, United States; orcid.org/0000-0003-1152-1912*

Gordon J. Miller – *Department of Chemistry, Iowa State University, Ames, Iowa 50011, United States; orcid.org/ 0000-0001-5717-8000*

Notes

The authors declare no competing financial interest.

■ ACKNOWLEDGMENTS

This work was financially supported by the Basic Science Research Program through the National Research Foundation of Korea (NRF) funded by the Ministry of Science and ICT (NRF-2021R1A2C1003661 and 2019R1A2C3005530). KK and PY acknowledge support from the U.S. Department of Energy, Office of Basic Energy Sciences, Division of Materials Science and Engineering (Grant No. DE-SC0022288).

■ REFERENCES

- (1) Hasan, M. N.; Wahid, H.; Nayan, N.; Mohamed Ali, M. S. Inorganic Thermoelectric Materials: A Review. *Int. J. Energy Res.* **2020**, *44*, 6170–6222.
- (2) Jia, N.; Cao, J.; Tan, X. Y.; Dong, J.; Liu, H.; Tan, C. K. I.; Xu, J.; Yan, Q.; Loh, X. J.; Suwardi, A. Thermoelectric materials and transport physics. *Materials Today Physics.* **2021**, *21*, 100519.
- (3) Hong, Y.; Yeon, S.; Yox, P.; Yunxiu, Z.; Choi, M.-H.; Moon, D.; Ok K. M.; Kim D.-H. Kovnir, K.; Miller, G. J.; You, T.-S. Role of Eu-Doping in the Electron Transport Behavior in the Zintl Thermoelectric $\text{Ca}_{5-x-y}\text{Yb}_x\text{Eu}_y\text{Al}_2\text{Sb}_6$ System. *Chem. Mater.* **2022**, *34*, 9903–9914.
- (4) Ohno, S.; Aydemir, U.; Amsler, M.; Pöhls, J. H.; Chanakian, S.; Zevalkink, A.; White, M. A.; Bux, S. K.; Wolverton, C.; Snyder, G. J. Achieving $zT > 1$ in Inexpensive Zintl Phase $\text{Ca}_9\text{Zn}_{4+x}\text{Sb}_9$ by Phase Boundary Mapping. *Adv. Funct. Mater.* **2017**, *27*, 1606361.
- (5) Yeon, S.; Shin, S.; Jo, H.; Thi, N. L.; Moon, D.; Kim, D.-H.; Ok, K. M.; You, T.-S. p-Type to n-Type Conversion through the “Bypass” Phase Transition in the Zintl-Phase Thermoelectric Materials. *Chem. Mater.* **2021**, *33*, 6761–6773.
- (6) Sa, H.; Lee, J.; Jo, H.; Moon, D.; Kim, M.; Ok, K. M.; You, T.-S. p-Type Double Doping and the Diamond-like Morphology Shift of the Zintl Phase Thermoelectric Materials: The $\text{Ca}_{11-x}\text{A}_x\text{Sb}_{10-y}\text{Ge}_z$ ($\text{A} = \text{Na}, \text{Li}; 0.06(3) \leq x \leq 0.17(5), 0.19(1) \leq y \leq 0.55(1), 0.13(1) \leq z \leq 0.22(1)$) System. *Inorg. Chem.* **2021**, *60*, 10124–10136.
- (7) Lee, J.; Shin, S.; Jo, H.; Shin, W. H.; Moon, D.; Ok, K. M.; You, T.-S. Two Steps to Improve the Thermoelectric Performance of the $\text{Ca}_{5-x}\text{Yb}_x\text{Al}_{2-y}\text{In}_y\text{Sb}_6$ System. *Inorg. Chem.* **2020**, *59*, 13572–13582.
- (8) Cordier, G.; Schäfer, H.; Stelter, M. New Zintl Phases with Chain Anions: On Ca_3AlSb_3

and $\text{Ca}_5\text{Al}_2\text{Bi}_6$. *Z. Naturforsch. B* **1984**, *39*, 727–732.

(9) Nam, G.; Choi, W.; Jo, H.; Ok, K. M.; Ahn, K.; You, T.-S. Influence of Thermally Activated Solid-State Crystal-to-Crystal Structural Transformation on the Thermoelectric Properties of the $\text{Ca}_{5-x}\text{Yb}_x\text{Al}_2\text{Sb}_6$ ($1.0 \leq x \leq 5.0$) System. *Chem. Mater.* **2017**, *29*, 1384–1395.

(10) Miller, G. J.; Schmidt, M. W.; Wang, F.; You, T.-S. Quantitative Advances in the Zintl-Klemm Formalism. In *Zintl Phases: Principles and Recent Developments*; Springer-Verlag: Berlin, 2011; pp 1–55.

(11) *APEX3*; Bruker AXS Inc.: Madison, WI, USA, 2016.

(12) *SAINT*; Bruker AXS Inc.: Madison, WI, USA, 2002.

(13) Sheldrick, G. M. *SADABS*; University of Göttingen: Göttingen, Germany, 2003.

(14) Shin, J. W.; Eom, K.; Moon, D. BL2D-SMC, the supramolecular crystallography beamline at the Pohang Light Source II, Korea. *J. Synchrotron Radiat.* **2016**, *23*, 369–373.

(15) Otwinowski, Z.; Minor, W. Processing of X-ray diffraction data collected in oscillation mode. *Methods Enzymol.* **1997**, *276*, 307–326.

(16) Gelato, L. M.; Parthe, E. *STRUCTURE TIDY* - A computer program to standardize crystal structure data. *J. Appl. Crystallogr.* **1987**, *20*, 139–143.

(17) Andersen, O. K. Linear methods in band theory. *Phys. Rev. B* **1975**, *12*, 3060–3083.

(18) Andersen, O. K.; Jepsen, O. Explicit, first-principles tight binding theory. *Phys. Rev. Lett.* **1984**, *53*, 2571–2574.

(19) Lambrecht, W. R. L.; Andersen, O. K. Minimal basis sets in the linear muffin-tin orbital method: Application to the diamond structure crystals C, Si, and Ge. *Phys. Rev. B* **1986**, *34*, 2439–2449.

(20) Jepsen, O.; Burkhardt, A.; Andersen, O. K. *The TB-LMTO-ASA Program* (ver. 4.7); Max-Planck-Institut für Festkörperforschung: Stuttgart, Germany, 1999.

- (21) Andersen, O. K.; Jepsen, O.; Glötzel, D. Canonical Description of the Band Structures of Metals. In *Highlights of Condensed Matter Theory*; Bassani, F., Fumi, F., Tosi, M., Eds.; Elsevier North Holland: New York, 1985; pp 65-72.
- (22) Jepsen, O.; Andersen, O. K. Calculated electronic structure of the sandwich d^1 metals LaI_2 and CeI_2 : Application of new LMTO techniques. *Z. Phys. B: Condens. Matter*. **1995**, *97*, 35–47.
- (23) Blöchl, P. E.; Jepsen, O.; Andersen, O. K. Improved tetrahedron method for Brillouin-zone integrations. *Phys. Rev. B* **1994**, *49*, 16223–16233.
- (24) Kim, H.-S.; Gibbs, Z. M.; Tang, Y.; Wang, H.; Snyder, G. J. Characterization of Lorenz number with Seebeck coefficient measurement. *APL Mater.* **2015**, *3*, 041506.
- (25) Zevalkink, A.; Toberer, E. S.; Zeier, W. G.; Flage-Larsen, E.; Snyder, G. J. Ca_3AlSb_3 : an inexpensive, non-toxic thermoelectric material for waste heat recovery. *Energy Environ. Sci.* **2011**, *4*, 510–518.
- (26) Zeier, W. G.; Zevalkink, A.; Schechtel, E.; Tremel, W.; Snyder, G. J. Thermoelectric Properties of Zn-Doped Ca_3AlSb_3 . *J. Mater. Chem.* **2012**, *22*, 9826–9830.
- (27) Cordier, G.; Schäfer, H. Ca_3AlAs_3 —Ein Intermetallisches Analogon Zu Den Kettensilicaten. *Angew. Chem.* **1981**, *93*, 474.
- (28) Verdier, P.; L'Haridon, P.; Mounaye, M.; Laurent, Y. Etude structurale de $\text{Ca}_5\text{Ga}_2\text{As}_6$. *Acta Crystallogr., Sect. B* **1976**, *32*, 726–728.
- (29) Shannon, R. D. Revised effective ionic radii and systematic studies of interatomic distances in halides and chalcogenides. *Acta Crystallogr., Sect. A: Cryst. Phys., Diffr., Theor. Gen. Crystallogr.* **1976**, *A32*, 751–767.
- (30) Lee, J.; Ahn, K.; Kim, K.; Jo, H.; Yoon, J. S.; Moon, D.; Shin, W. H.; Ok, K. M.; You, T.-S. Effect of Rare-Earth Metals Substitution for Ca on the Crystal Structure and Thermoelectric Properties of the $\text{Ca}_{11-x}\text{RE}_x\text{Sb}_{10-y}$ System. *Cryst. Growth Des.* **2019**, *19*, 3498–3508.

- (31) Kim, K.; Lee, J.; Shin, S.; Jo, H.; Moon, D.; Ok, K. M.; You, T.-S. Chemical Driving Force for Phase-Transition in the $\text{Ca}_{2-x}\text{RE}_x\text{CdSb}_2$ (RE = Yb, Eu; $0.11 (1) \leq x \leq 1.36 (2)$) System. *Cryst. Growth Des.* **2020**, *20*, 746–754.
- (32) Kim, H. G.; Tran, T. T.; Choi, W.; You, T.-S.; Halasyamani, P. S.; Ok, K. M. Two New Non-centrosymmetric $n = 3$ Layered Dion-Jacobson Perovskites: Polar $\text{RbBi}_2\text{Ti}_2\text{NbO}_{10}$ and Nonpolar $\text{CsBi}_2\text{Ti}_2\text{TaO}_{10}$. *Chem. Mater.* **2016**, *28*, 2424–2432.
- (33) Baranets, S.; Bobev, S. $\text{Ca}_{14}\text{AlBi}_{11}$ —a New Zintl Phase from Earth-Abundant Elements with a Great Potential for Thermoelectric Energy Conversion. *Mater. Today Adv.* **2020**, *7*, 100094.
- (34) Emsley, J. *The Elements*; Oxford University Press: New York, 1989.
- (35) Cao, Q.-G.; Zhang, H.; Tang, M.-B.; Chen, H.-H.; Yang, X.-X.; Grin, Y.; Zhao, J.-T. Zintl Phase $\text{Yb}_{1-x}\text{Ca}_x\text{Cd}_2\text{Sb}_2$ with Tunable Thermoelectric Properties Induced by Cation Substitution. *J. Appl. Phys.* **2010**, *107*, 053714.
- (36) Nam, G.; Choi, W.; Lee, J.; Lim, S. J.; Jo, H.; Ok, K. M.; You, T.-S. Effect of Multisubstitution on the Thermoelectric Performance of the $\text{Ca}_{11-x}\text{Yb}_x\text{Sb}_{10-y}\text{Ge}_z$ ($0 \leq x \leq 9$; $0 \leq y \leq 3$; $0 \leq z \leq 3$) System: Experimental and Theoretical Studies. *Inorg. Chem.* **2017**, *56*, 7099–7110.
- (37) Perez, C. J.; Cerretti, G.; Wille, E. L. K.; Devlin, K. P.; Grewal, N. S.; Justl, A. P.; Wood, M.; Bux, S. K.; Kauzlarich, S. M. Evolution of Thermoelectric Properties in the Triple Cation Zintl Phase: $\text{Yb}_{13-x}\text{Ca}_x\text{BaMgSb}_{11}$ ($x = 1-6$). *Chem. Mater.* **2021**, *33*, 8059–8069.
- (38) Chen, C.; Xue, W.; Li, S.; Zhang, Z.; Li, X.; Wang, X.; Liu, Y.; Sui, J.; Liu, X.; Cao, F.; Ren, Z.; Chu, C. W.; Wang, Y.; Zhang, Q. Zintl-Phase Eu_2ZnSb_2 : A Promising Thermoelectric Material with Ultralow Thermal Conductivity. *Proc. Natl. Acad. Sci. U.S.A.* **2019**, *116*, 2831–2836.

(39) Cooley, J. A.; Promkhan, P.; Gangopadhyay, S.; Donadio, D.; Pickett, W. E.; Ortiz, B. R.; Toberer, E. S.; Kauzlarich, S. M. High Seebeck Coefficient and Unusually Low Thermal Conductivity Near Ambient Temperatures in Layered Compound $\text{Yb}_{2-x}\text{Eu}_x\text{CdSb}_2$. *Chem. Mater.* **2018**, *30*, 484–493.

TOC Only

